Supporting Information for:

SELF-OPTIMIZING PHOTOELECTROCHEMICAL GROWTH OF NANOPATTERNED SE-TE FILMS IN RESPONSE TO THE SPECTRAL DISTRIBUTION OF INCIDENT ILLUMINATION

AZHAR I. CARIM[1], NICOLAS A. BATARA[2], ANJALI PREMKUMAR[2],

HARRY A. ATWATER[2-5] AND NATHAN S. LEWIS[1,3-5*]

[1]Division of Chemistry and Chemical Engineering

[2]Division of Engineering and Applied Sciences

[3]The Joint Center for Artificial Photosynthesis

[4]Kavli Nanoscience Institute

[5]Beckman Institute

California Institute of Technology

Pasadena, CA 91125

*Corresponding Author: nslewis@caltech.edu

S1. Contents

This document contains a description of the experimental and modeling/simulation methods utilized in this work (Sections S2 and S3), additional scanning-electron micrographs (Section S4), an analysis of the elemental composition of the photoelectrodeposits (Section S5), and a list of associated references (Section S6).

S2. Experimental Methods

Materials and Chemicals $(CH_3)_2CO$ (ACS Grade, BDH), H_2SO_4 (ACS Reagent, J. T. Baker), HF (49 %, Semiconductor Grade, Puritan Products), In (99.999 %, Alfa Aesar), Ga (99.999 %, Alfa Aesar), SeO_2 (99.4 %, Alfa Aesar), and TeO_2 (99+ %, Sigma-Aldrich) were used as received. H_2O with a resistivity ≥ 18.2 MΩ cm (Barnstead Nanopure System) was used throughout. n^+-Si(111) (0.004 – 0.006 Ω cm, As-doped, 400 ± 15 μm, single-side polished, Addison Engineering) was used as a substrate for deposition. Flash-Dry Silver Paint (SPI Supplies), Double/Bubble Epoxy (Hardman) and nitrocellulose-based nail polish were used to assemble the Si working electrodes.

Electrode Preparation One end of a Sn-coated Cu wire (22 AWG) was bent to form a small, flat coil and the wire was then threaded through glass tubing (6 mm O. D.) such that the coil was just outside the tubing. Epoxy was applied to seal the end of the tube from which the coil protruded. Square Si wafer sections (ca. 5 mm by 5 mm) were cut and a eutectic mixture of Ga and In was scratched into the unpolished surfaces with a carbide scribe. The wire coil was then contacted to the unpolished surface and affixed with Ag paint. Nail polish was applied to insulate the unpolished face, the wire-coil contact and the exposed wire between the coil and epoxy seal. Immediately before deposition, the Si surface of each electrode was cleaned with $(CH_3)_2CO$, and then the Si section of the electrode was immersed in a 49 wt. % solution of HF(aq) for ~ 10 s, to remove any surficial SiO_x from the Si. The electrode was then rinsed with H_2O, and then dried under a stream of N_2(g).

Photoelectrochemical Deposition All photoelectrochemical deposition was a carried out using a Bio-Logic SP-200 potentiostat. Deposition was performed in a single-compartment glass cell with a quartz window. A three-electrode configuration was utilized with a graphite-rod

counter electrode (99.999 %, Sigma-Aldrich) and a Ag/AgCl reference electrode (3 M KCl, Bioanalytical Systems). Films were deposited from an aqueous solution of 0.0200 M SeO_2, 0.0100 M TeO_2, and 2.00 M H_2SO_4. Deposition was effected by biasing the illuminated n^+-Si electrode potentiostatically at -0.40 V vs. Ag/AgCl for 2.50 min at room temperature. After deposition, the electrode was immediately removed from the cell, rinsed with H_2O, and then dried under a stream of N_2(g). The Si substrate with top-facing Se-Te film was mechanically separated from the rest of the electrode assembly. The nitrocellulose-based insulation, as well as the majority of the Ag paint and In-Ga eutectic, were then removed mechanically.

Alloying Se with Te reduces the band gap of the material, enhancing light absorption.[1] The energetically favorable co-deposition of Se and Te reduces the influence of the solution composition on the generated alloy composition. If the alloy composition could be a varied, a change in the periodicity of the morphology that occurs as a result of photoelectrochemical preparation may be observed in response to a change in the relevant optical properties, such as the refractive index, of the material. We have not explicitly investigated the effects of the forced convection in the solution on the nature of the deposit, since the purpose of this study was to investigate the effects of varying the interaction between the light field and growing matter in the deposit under conditions similar to those used in prior work in the absence of specifically tuned spectral distributions of the incident illumination.

Electrode Illumination Illumination for the majority of the photoelectrochemical depositions was provided by narrowband diode (LED) sources (Thorlabs) with respective intensity-weighted λ_{avg} values and spectral bandwidths (FWHM) of 461 nm and 29 nm (M470L2), 630 nm and 18 nm (M625L3), and 843 nm and 30 nm (M850L3). Additionally, a HeNe laser (Aerotech LSR5P) emitting at 632.8 nm in a TEM_{00} mode with linear polarization, a

broadband diode (LED, Thorlabs MBB1L3) with a relatively flat intensity profile between 500 and 750 nm (λ_{avg} = 646 nm) and a spectral bandwidth (FWHM) of 280 nm, and an ELH-type tungsten-halogen lamp (Phillips 13096) with a λ_{avg} value of 640 nm and a spectral bandwidth (FWHM) of 420 nm, were also used as light sources. The output of each diode source was collected and collimated with an aspheric condenser lens (Ø30 mm, f = 26.5 mm). The HeNe laser was fitted with a 10x beam expander (Melles-Griot) to create a spot that overfilled the working electrode. For experiments involving simultaneous illumination with two different wavelengths, a dichroic filter (Edmund Optics #69-900 or #69-219) was utilized. Both sources were incident upon a filter surface at an angle of 45 degrees from the surface normal, generating coaxial output. A dichroic film polarizer (Thorlabs LPVISE2X2 or LPNIRE200-B) was used to polarize the illumination from all of the narrowband diode sources. For experiments involving simultaneous illumination from two sources, the polarizer was placed after the dichroic filter to ensure that all of the light that reached the electrode shared a single polarization vector. Illumination from the broadband diode and from the tungsten-halogen lamp was polarized using an ultra-broadband wire-grid polarizer (Thorlabs WP25M-UB). No polarization optic was used in conjunction with the HeNe laser. A 1500 grit ground-glass (N-BK7) diffuser was placed immediately in front of the photoelectrochemical cell to ensure spatial homogeneity of the illumination. The light intensity incident on the electrode was measured by placing a calibrated Si photodiode (Thorlabs FDS100) in the place of an electrode assembly in a photoelectrochemical cell with electrolyte, and measuring the steady-state current response of that Si photodiode. Depositions that utilized a single diode as the illumination source were performed with a light intensity of 25.0 mW cm^{-2} at the electrode. Depositions with the HeNe laser were performed with a light intensity of 10.0 mW cm^{-2}. Depositions with the halogen lamp

were performed with a light intensity of 50.0 mW cm^{-2}. Depositions utilizing the diodes with λ_{avg} values of 630 nm and 461 nm in conjunction were performed with a total light intensity of 25.0 mW cm^{-2}. Depositions utilizing the diodes with λ_{avg} values of 630 nm and 843 nm in conjunction were performed with a total light intensity of 50.0 mW cm^{-2}.

Microscopy Scanning electron micrographs (SEMs) were obtained with a FEI Nova NanoSEM 450 at an accelerating voltage of 5.00 kV with a working distance of 5 mm and an in-lens secondary electron detector. Micrographs obtained for quantitative Fourier analysis were acquired with a resolution of 172 pixels μm^{-1} over ca. 120 μm^2 areas. Micrographs utilized to produce display figures were acquired with a resolution of 344 pixels μm^{-1} over ca. 8 μm^2 areas.

Energy-dispersive X-ray Spectroscopy Energy dispersive X-ray spectroscopy (EDS) was performed in the SEM using an accelerating voltage of 15.00 kV and a working distance of 12 mm. An Oxford Instruments X-Max silicon drift detector was utilized. Spectra were collected in the range of 0 to 10 keV and quantitative film compositions were derived from these spectra using the “INCA” software package (Oxford Instruments).

S3. Modeling and Simulation Methods

Simulation of Film Morphology The growths of the photoelectrochemically deposited films were simulated with an iterative growth model wherein electromagnetic simulations were first used to calculate the local photocarrier-generation rates at the film surface. Then, mass addition was simulated via a Monte Carlo method wherein the local photocarrier-generation rate weighted the local rate of mass addition along the film surface.

Growth simulations began with a bare, semi-infinite planar Si substrate. In the first step, the light-absorption profile under a linearly polarized, plane-wave illumination source was calculated using full-wave finite-difference time-domain (FDTD) simulations with periodic boundary conditions along the substrate interface. In the second step, a Monte Carlo simulation was performed in which an amount of mass, equaling that of a 15 nm planar layer covering the simulation area, was added to the upper surface of the structure with a probability *F*:

$$F(G) = \left[1 + G(\mathrm{n}_0\tau_p + \mathrm{p}_0\tau_n) + G^2\frac{\tau_p\tau_n}{\mathrm{n}_i^2}\right]\prod_{i=1}^{3}\frac{x_i}{r_i} \quad \textbf{(Equation 1)}$$

where *G* is the spatially-dependent photocarrier generation rate at the deposit-solution interface, n_i is the intrinsic carrier concentration, n_0 is the electron concentration, p_0 is the hole concentration, τ_n is the electron lifetime, τ_p is the hole lifetime, *x* is the fraction of i^{th} nearest neighbors occupied in the cubic lattice, and r_i is the distance to the i^{th} nearest neighbor. The multiplicative sum in the definition of this probability (Equation 1) serves to reduce the surface roughness of the film so as to mimic the experimentally observed surface roughness.

After the initial Monte Carlo simulation, the absorbance of the new, structured film was then calculated in the same manner as for the initial planar film, and an additional Monte Carlo simulation of mass addition was performed. This process of absorbance calculation and mass

addition was repeated for a total of 30 iterations.

Simulation of Spatial Concentration of Light Absorption The spatial concentration of light absorption in idealized versions of the lamellar-type structure generated by photoelectrochemical growth was investigated via a series of full-wave electromagnetic simulations.

Figure S1 provides a schematic of the simulation area. The idealized structure, from bottom to top, consisted of a semi-infinite Si substrate, a 100 nm conformal Se-Te layer, and a 400 nm tall Se-Te lamella with a hemispherical upper boundary. The lamella was separated into top and bottom regions at the height at which the surface normal to the hemispherical tip was 45 degrees from horizontal. A figure of merit, Ξ, was defined as the ratio of number of absorbed photons at the top solid/solution interface to the number of absorbed photons at the bottom solid/solution interface. The value of Ξ was thus proportional to the degree of light concentration in the top of the lamellar structure. Calculation of Ξ was limited to photons that were absorbed within 10 nm of the interface. Ξ was calculated for lamellar periods ranging from 100 to 400 nm. The width of structures in the simulations was set as the product of the lamellar period and the empirically derived filling fraction for the illumination condition under analysis (quantified by contrast-thresholding the same SEMs utilized for Fourier analysis).

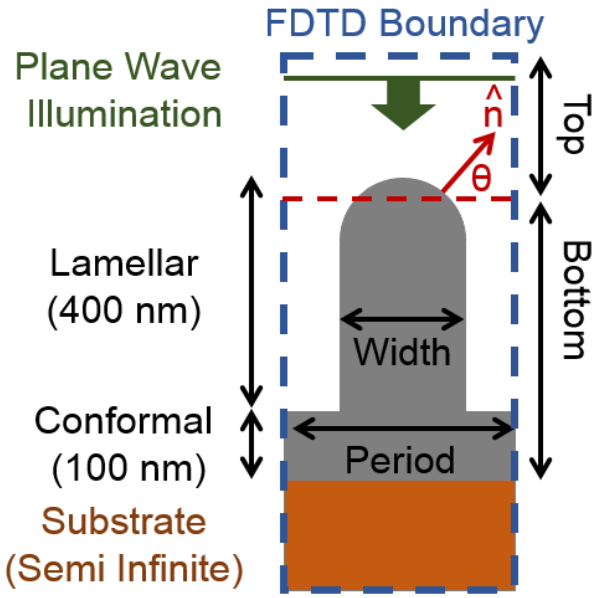

Figure S1. Diagram of simulation area containing an idealized lamellar structure utilized for calculations of spatial concentration of light absorption. A 400 nm tall lamellar deposit, a 100 nm conformal deposit, and a semi-infinite substrate were considered, with each component atop the next. The lamella was divided into top and bottom segments at the height at which the surface normal of the tip ($\hat{n}$) was at an angle $\theta = 45$ degrees from the horizontal. Periodic boundary conditions were utilized. Plane-wave illumination incident at the top of the structure and with a propagation direction oriented along the lamellar axis was considered.

General Parameters Se–Te films were assumed to be undoped (i.e. $n_0 = p_0 = n_i$) and a value of $n_i = 10^{10}$ cm^{-3} was used for the intrinsic carrier concentration.[2] A value of 1 μs was used for both the electron and hole lifetimes.[3] Previously measured values of the complex index of refraction for Se-Te were utilized.[4] A value of n = 1.33 was used as the refractive index of the electrolyte regardless of wavelength.[5] Illumination intensities identical to those used experimentally (see Section S2) were used in the simulations. Illumination spectral profiles for each relevant source were the same as those presented in Figure 1 and Figure 3 (see main text) for the FOM calculations described above. Simulations of the film morphology utilized the peak intensity wavelength of the experimental sources described in Section S2. The electric field vector of the illumination was oriented parallel to the substrate. A two-dimensional square mesh with a lattice constant of 1 nm was used for the simulations. All FDTD simulations were

performed using the “FDTD Solutions” software package (Lumerical).

S4. Additional Scanning Electron Micrographs

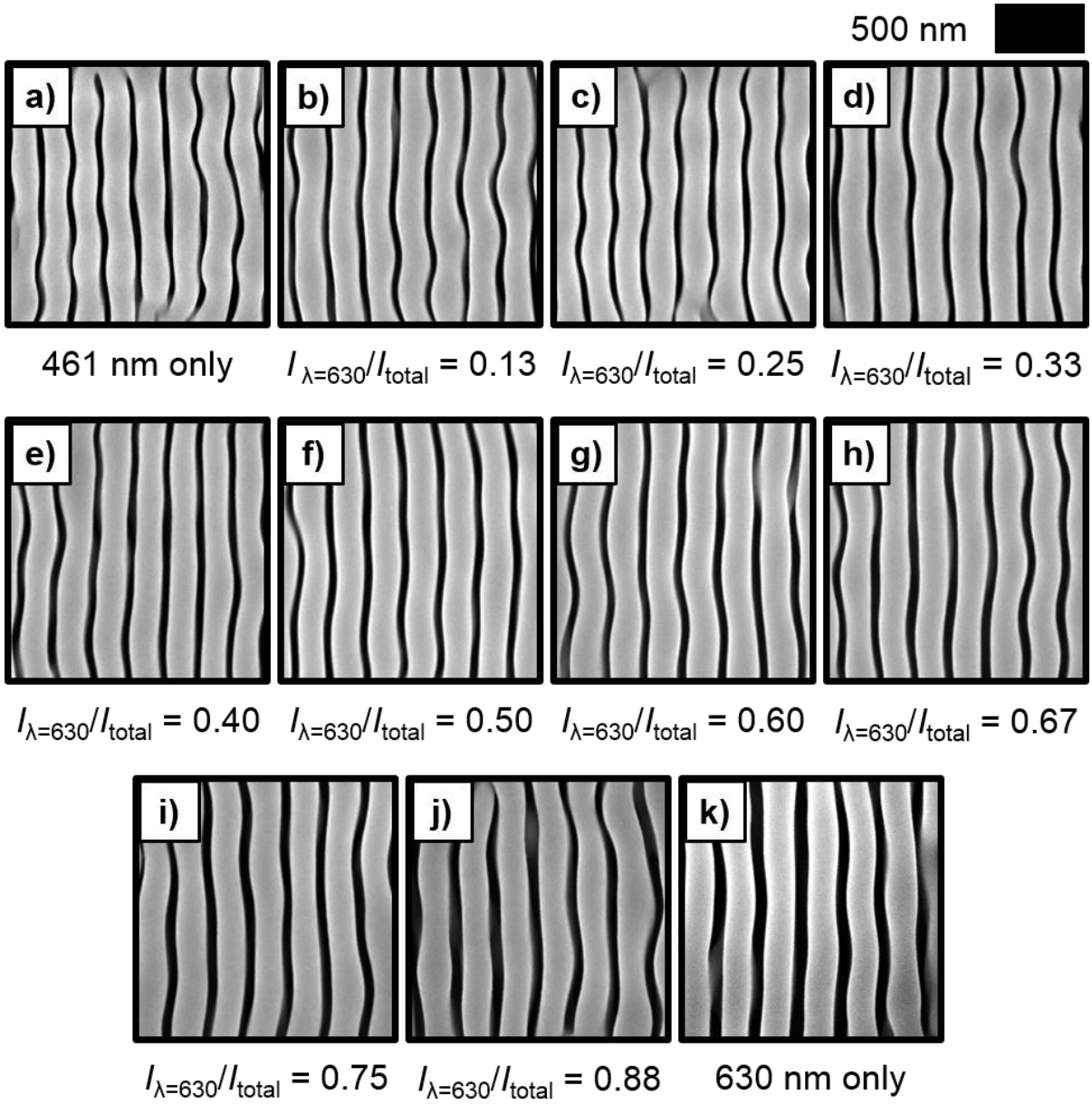

Figure S2. SEMs representative of resultant photoelectrodeposit from simultaneous illumination with LED sources with λ_{avg} values of 461 nm and 630 nm (spectral profiles as indicated in Figure 3(a)) with the indicated intensity ratio between the two sources.

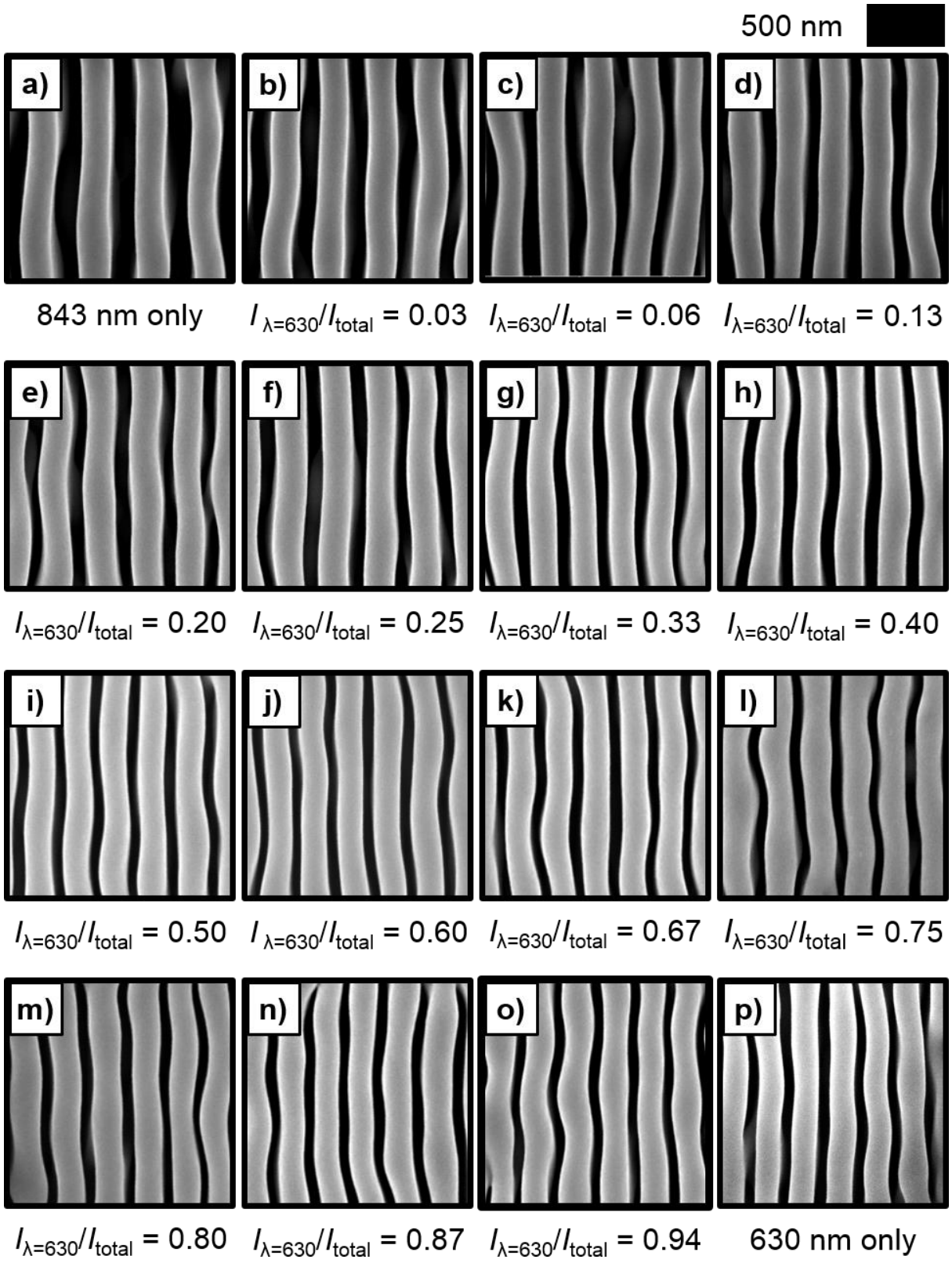

Figure S3. SEMs representative of resultant photoelectrodeposit from simultaneous illumination with LED sources with λ_{avg} values of 843 nm and 630 nm (spectral profiles as indicated in Figure 3(e)) with the indicated intensity ratio between the two sources.

S5. Elemental Composition of Photoelectrodeposits

The elemental composition of all of the photoelectrodeposits was analyzed using energy-dispersive X-ray spectroscopy (EDS). All analyzed films were found to be wholly composed of Se and Te. Photoelectrodeposits generated using the HeNe laser (λ_{avg} = 633 nm) were found to on average to have compositions of 38 atomic % Se (remainder Te). Photoelectrodeposits generated with the narrowband LED with λ_{avg} = 630 nm, the broadband LED with λ_{avg} = 646 nm, and the tungsten-halogen lamp with λ_{avg} = 640 nm were found to on average have compositions of 37, 37 and 39 atomic % Se, respectively. The uncertainty inherent in the EDS measurement was ~5 atomic % and thus the differences between these values are not significant. Figure S4(a) presents a plot of the elemental composition (in terms of atomic % Se) of the photoelectrodeposits generated with simultaneous illumination at 461 nm and 630 nm as a function of the source composition (in order of increasing 630 nm content). Figure S4(b) presents analogous data pertaining to the photoelectrodeposits generated with simultaneous illumination at 630 nm and 843 nm. In both cases, photoelectrodeposits were found to on average have compositions of 37 atomic % Se and all the average compositions were found to range between 37 and 39 atomic % Se. Again, these values were within experimental uncertainty and as such these values are statistically equivalent. Thus, no variation in photoelectrodeposit elemental composition was found between any of the experimental parameters investigated in this work.

Additionally, EDS analysis was also performed on several different spatial locations on each photoelectrodeposit. The variability in observed elemental composition was ~ 2 atomic % Se. This variability is less than the experimental uncertainty, indicating that the photoelectrodeposits are spatially conformal within the certainty afforded by EDS analysis.

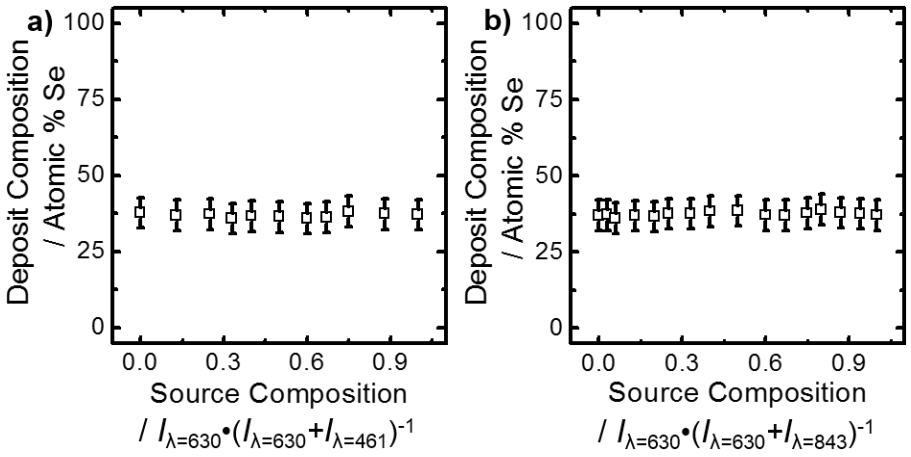

Figure S4. (a) and (b) Plots of the elemental composition of the photoelectrodeposit in terms of atomic % of Se as a function of the fraction of the total intensity provided by the 630 nm source utilized during growth. Photoelectrodeposits were composed wholly of Se and Te.

S6. References

1. Reddy, K. V.; Bhatnagar, A. K. *J. Phys. D: Appl. Phys.* **1992**, *25*, 1810-1816.
2. El-Korashy, A.; El-Zahed, H.; Zayed, H. A.; Kenawy, M. A. *Solid State Commun.* **1995**, *95*, 335-339.
3. Mott, N. F.; Davis, E. A., *Electronic Processes in Non-Crystalline Materials*. 2 ed.; Oxford University Press: New York, 1971.
4. Sadtler, B.; Burgos, S. P.; Batara, N. A.; Beardslee, J. A.; Atwater, H. A.; Lewis, N. S. *Proc. Natl. Acad. Sci. U. S. A.* **2013**, *110*, 19707-12.
5. Hale, G. M.; Querry, M. R. *Appl. Opt.* **1973**, *12*, 555-563.